ChemComm

Accepted Manuscript

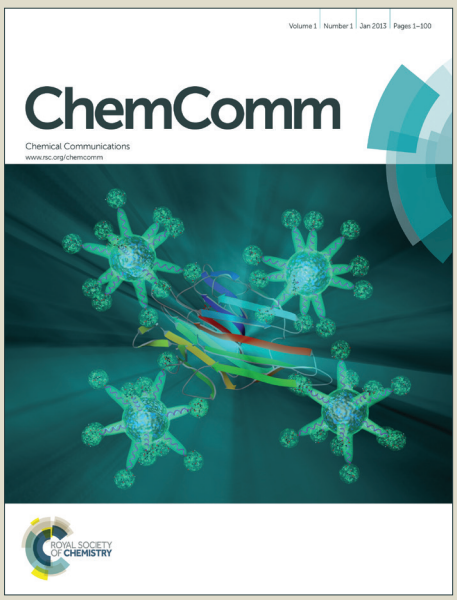

ROYAL SOCIETY OF CHEMISTRY

www.rsc.org/chemcomm

Journal Name

COMMUNICATION

Liquor ammonia mediated V(V) insertion in thin Co_3O_4 sheet for improved pseudocapacitor with high energy density and high specific capacitance value

Received 00th January 20xx,
Accepted 00th January 20xx

DOI: 10.1039/x0xx00000x

www.rsc.org/

Ramkrishna Sahoo[a], Anindita Roy[a], Soumen Dutta[a],Chaiti Ray[a], Teresa Aditya[a], Anjali Pal[b] and Tarasankar Pal*[a]

Ultrathin 2D Co_3O_4 and $Co_3V_2O_8$ nanosheets have been produced from our modified hydrothermal (MHT) technique. Both the materials have proved to be extraordinary electrode materials for pseudocapacitance. The neat nanosheets of Co_3O_4 and $Co_3V_2O_8$ exhibit record specific capacitance value 1256 F/g and 4194 F/g at 1 A/g current density, respectively.

Supercapacitors with fast charge-discharge property, large cyclic stability, high power density and large coulombic efficiency have drawn attention for practical utility in electrical vehicles, advanced charge storage devices etc.[1] Limitation of supercapacitors lies always with low energy density compared to Li-ion batteries. Energy density can be increased by increasing specific capacitance value (C) and applied cell voltage (V). To increase the applied cell voltage generally solid state asymmetric electrodes are designed which consist of battery-like and capacitor-like electrodes.[2] Between the electrochemical double layer capacitor and pseudocapacitor, the latter has become more popular for its high specific capacitance value and fast charge-discharge property due to rapid reversible multi-electron relay via Faradic redox reactions.[3] For this purpose many redox active materials such as MnO_2,[4] $Ni(OH)_2/NiO$,[3,5] $Co_3O_4/Co(OH)_2$[6,7] etc. have been used. The pseudocapacitor, in most cases, faces major problem as the materials involve only the surface layers again which are often discontinuous and also bear non-participating bulk. Thus utility of the active material in case of pseudocapacitor becomes less effective. Now a days fabrication of electrode for charge storage with mixed oxides has been proved to be promising materials due to their synergistic effect.[8-15] Among the transition metal oxides researchers are now interested towards vanadium oxide, due to its large number of oxidation state, high abundance, non-toxicity etc.[9-15] All these effects are supplemented due to the maximum utilization of active material which increases the quality of the pseudocapacitor. Ultrathin two-dimensional (2D) nanosheets are proved to be very significant in practice due to their remarkable chemical as well as physical properties, such as high molecular thickness, provision of large number of active sites, good structural stability, short diffusion path length, etc.[4,7,16,17]

By keeping the above considerations and limitations in mind, here in this communication we report the preparation of two different cobalt based nanosheets C_1 and C_2 (Co_3O_4 and $Co_3V_2O_8$, respectively) using our laboratory developed modified hydrothermal technique (MHT)[18] in liquor ammonia solution (supporting information provides discussion). The as-synthesized materials are used as electrochemical supercapacitor in a three-electrode system where glassy carbon has been used as the working electrode. The mixed oxide electrode material exhibits very high specific capacitance, high stability and high energy density value.

Interestingly, we have obtained thin nanosheets for both Co_3O_4 and $Co_3V_2O_8$ samples from MHT. The crucial stages of the synthetic strategy are temperature and usage of liquor NH_3 as the hydrolyzing agent. There are some reports of $Co_3V_2O_8$ nanostructure preparation but none of them reported sheet like morphology.[9-13] Figure S1 demonstrates the schematic presentation of the synthesis of C_2 sample. A homogeneous alkalinisation of precursor salt solutions with strong ammonia hydrolyses metal salts under MHT. The formation of ultrathin nanosheets is dominated by self-assembly and oriented attachment mechanism.[19] In the oriented attachment process nanoparticles rotate to optimize the crystallographic orientation at low surface energy. Finally at the interface irreversible attachment occurs with each other through later atom-by-atom addition.[20] Again, ammonia by its intrinsic driving force, presumably through H-bonding, initiates 2D anisotropic growth of the materials. NH_4^+ from aqueous ammonia has a significant role to modify the surface of the metal oxide nanoparticles. Different binding ability and hydrogen bond formation of ammonium ion with the metal ions (here Co^{2+} and V^{5+}) may be the reason behind the variation in the surface energies of the metal oxide

[a] Department of Chemistry Indian institute of Technology, Kharagpur, India. Email: tpal@chem.iitkgp.ernet.in
[b] Department of Civil Engineering Indian institute of Technology, Kharagpur, India
† Footnotes relating to the title and/or authors should appear here.
Electronic Supplementary Information (ESI) available: [details of any supplementary information available should be included here]. See DOI: 10.1039/x0xx00000x

nanocrystals. During this process, at a particular condition i.e., at low surface energy metal oxide nanoparticles assemble in a symmetric configuration which leads to the formation of nanosheet. Finally, MHT condition dehydrates the product of hydrolysis to oxide.[21] Other common hydrolyzing agents were unsuccessful in this endeavor to produce sheets.

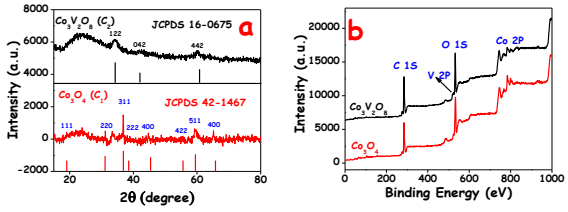

Fig. 1 a) XRD and b) wide range XPS of the C_1 and C_2 samples.

To characterize the as-synthesized nanosheets useful characterization techniques have been used. Figure 1a displays the XRD patterns of the samples C_1 and C_2 which matches well with the reported Co_3O_4 and $Co_3V_2O_8$ results.[6],[13], Red line (C_1) in Figure 1a indicates the face centered cubic phases of Co_3O_4 (JCPDS 42-1467) with cell constants values, a = b = c = 0.8083 nm where diffraction peaks with their crystal planes are visible.[6] On the other hand, black line (C_2) confirms the cubic phase of $Co_3V_2O_8$ (JCPDS 16-0675) with their crystal planes and characteristic diffraction peaks.[13]

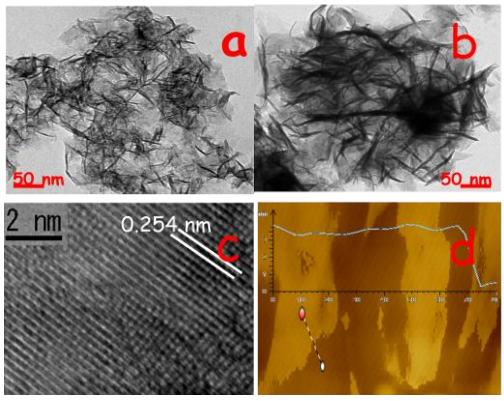

Fig. 2 TEM images of a) C_2 and b) C_1 samples, respectively. c) HRTEM image and d) AFM image and thickness profile of C_2 sample.

Wide range XPS of C_1 and C_2 samples (Figure 1b) indicates that C_1 is comprised of Co and O only and that of C_2 is with Co, V and O. Figure S2a also confirms that V is present in C_2 sample. Narrow range XPS of C_1 and C_2 (Figure S2b and c) demonstrates Co 2p, V 2p regions. For sample C_1, the Co $2p_{1/2}$ and Co $2p_{3/2}$ are located at 797.5 eV and 781.8 eV, respectively which authenticates that C_1 is Co_3O_4.[22] On the other hand for C_2 the Co $2p_{1/2}$ and Co $2p_{3/2}$ are positioned at 796.5 eV and 780.7 eV, respectively together with a strong satellite peak, characteristic of Co^{2+}, for sample C_2. The V $2p_{1/2}$ and V $2p_{3/2}$ positioned at 517.1 eV and 523 eV justify Co^{2+} and V^{5+} in C_2 implying it a $Co_3V_2O_8$.[10] EDS result also confirms that C_2 is composed of Co, V and O (Figure S3). Field emission scanning electron microscopic (FESEM, Figure S4a,b), transmission electron microscopic (TEM, Figure 2a,b), scanning transmission electron microscopic (STEM, Figure S4c,d) and atomic force microscopic (AFM, Figure S4e,f) analyses clearly reveal the ultrathin morphology for both the as-synthesized Co_3O_4 (C_1) and $Co_3V_2O_8$ (C_2) samples. Figure 2c shows lattice spacing of C_2 sample, bearing interplaner distance of 0.254 nm for (122) plane and that of C_1 appears at 0.284 nm for (220) plane (Figure S5a), which also validate that C_1 and C_2 are Co_3O_4 and $Co_3V_2O_8$, respectively. AFM measurement reveals the actual thickness of C_1 and C_2 samples which are 4.5 nm and 3.5 nm as observed from Figure S5b and Figure 2d, respectively. Elemental area mapping from STEM image confirms that C_1 is with Co and O only (Figure S6) and C_2 is composed of Co, V and O (Figure S7). N_2 adsorption-desorption isotherm of C_1 and C_2 samples were analyzed at 77 K in the region of relative pressure 0 to 1 (P/P_0) (figure S8). The BET surface area and pore diameter of the C_1 sample is 70 m^2/g and 4.02 nm respectively and that of C_2 sample is 76 m^2/g and 4.1 respectively, i. e., both the materials are mesoporous in nature.

Here we have used both the as-synthesized metal oxides as electrode materials for a pseudocapacitor. Both the samples inherit very high specific capacitance value, moderate rate capability, long range stability, high energy and power density. The total experiment has been carried out in 3M KOH solution. Figure 3a represents the cyclic voltammetry (CV) curve for C_1 and C_2 samples in the potential range -0.2 V to 0.4 V at the scan rate of 10 mV/s. In both the cases two pairs of redox peaks appear. The redox peaks indicate the involvement of two quasi-reversible electron transfer redox processes with the applied voltage. The reaction signatures are as follows:[23,24]

Anodic scan,

$Co^{2+} + 3OH^- = CoOOH + H_2O + e$ 1

$CoOOH + OH^- = CoO_2 + H_2O + e$.....2

Cathodic scan,

$CoO_2 + H_2O + e = CoOOH + OH^-$ 3

$CoOOH + H_2O + e = Co^{2+} + 3OH^-$ 4

It can be spelt out that, in alkaline medium $Co_3V_2O_8$ as well as Co_3O_4 react through Co (II) ↔ Co (III) ↔ Co (IV) redox stages. These faradic redox reactions are the reasons behind the mechanism of charge storage by the as-synthesized materials (pseudocapacitive nature).[23,24] Due to these redox reaction the peak shaped CV curves are produced.[23,24] The pseudocapacitive nature is very much different from electrical double layer capacitor (EDLC), as EDLC produces rectangular shaped CV curve.[24] Figure S9a,b illustrates that with the increase in scan rate the current density for both the samples increases. This is due to the fact that at high scan rate diffusion of OH^- ion is high and pronounced. From Figure S9a,b it is also observed that the anodic peaks and the cathodic peaks are not symmetrical. This indicates kinetic irreversibility of the material which occurs owing to the ohmic resistance and polarization during the redox reactions.[23] As per Figure 3b, the nonlinear charge-discharge curve for C_1 and C_2 again approves that, C_1 and C_2 exhibit pseudocapacitance in KOH electrolyte. The as-synthesized ultrathin nanosheets showed specific capacitance value 1256 F/g and 4194 F/g at 1 A/g current density for C_1 and C_2, respectively.

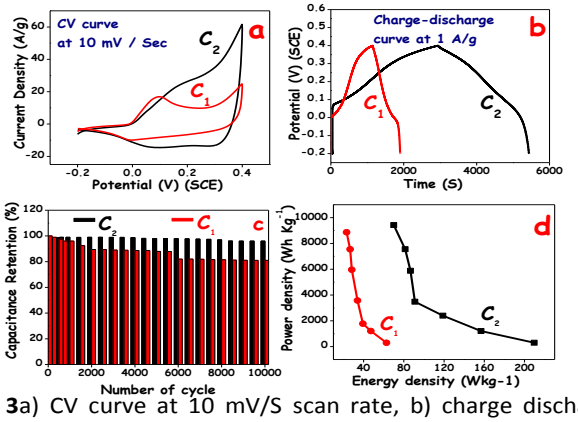

Fig. 3a) CV curve at 10 mV/S scan rate, b) charge discharge curve at 1 A/g, c) percentage specific capacitance retention after 10000 cycles and d) Ragone plot for C_1 and C_2 sample.

Recently, researchers have tried to develop advanced pseudocapacitor materials with high specific capacitance value from different techniques through synthesis of sheet like materials, doping and also addition of redox active materials with the electrolyte.[25-28] Here In this case we have obtained an excellent specific capacitance value from our ultrathin 2D $Co_3V_2O_8$ (C_2) only in aq. KOH electrolyte, without adding any redox active agent. The specific capacitance value of the as-synthesized C_1 is also superior than the recently reported Co_3O_4.[6,8,22,29] Table S1 represents the specific capacitance of the reported Co_3O_4 and other electrode materials where most of them bear sheet like morphology.

Table S2 contains the specific capacitance values of C_1 and C_2 at different current densities. We have checked the rate up to very high current density (30 A/g) for both the materials. At 30 A/g the specific capacitance values for C_1 and C_2 are 461 and 1400 F/g, respectively, i.e., at this current density the capacitance retention for C_1 is 36.71 % and that of C_2 is 33.34 %. As a pseudocapacitor these rate capability values are not bad at such high current density (here we did not use any carbonaceous material to increase the electrical conductivity[30,31]). At high current density C_1 shows high rate capability than C_2. This anomaly may be due to the high surafce activation of C_1 compared to C_2 at high current density. For pseudocapacitor, redox reactions occur at the electrode-electrolyte interface and electrolyte can diffuse to ~20 nm depth of the active material.[32] In our case thickness of both the materials is <5 nm and thus involvement of the whole surface as active material is understandable. Hence, ultrathin flat structures of both the materials make the ion diffusion process fast, extremely facile due to whole body participation of the active material. On the other hand mesoporous nature on the nanosheets increases the wettability of the elctrode, and facilitates the fast ion trasport which in turn increases the rate capability.[33] Figure S10a,b display the charge-discharge curve of C_1 and C_2 electrode materials at different current densities and Figure 3c demonstrates the stability of C_1 and C_2 at 30 A/g current density after 10000 cycles of charge-discharge. From this graphical presentation it is clear that after 10000 cycles C_1 retains 81% of its specific capacitance and whereas the same in case of C_2 is 96%, i.e. synergestic effect of cobalt and vanadium oxide in C_2 sample makes it stab[le] electrode for a pseudocapacitor. This cyclic durability of th[e] materials is essential for practical purpose. The kinet[ic] irreversibility of the materials is further substantiated from th[e] measured coulombic efficiency (η). Coulombic efficiency [is] governed by the quantitative charging time (t_C) and discharging time (t_D). The smaller the Δt, lower the kinet[ic] irreversibility and higher the accessibility of the surface for the OH^- ion.[24] In our case, for C_2, η value increases from 88% t[o] ~100% when current density increases from 1 A/g to 20 A/g, and for C_1, η values increase from 67% to ~100% when current density increases from 1 A/g to 30 A/g. Increase in η to such [a] large extent illustrates the structural activation and, hig[h] reversibility with the progress of charge discharge cycle.[2] Structural activation during charge-discharge cycle in such high current density provides much more involvement of th[e] interfacial ions which facilitates the mass transfer.[34] It [is] observed that at 1 A/g, η for C_2 is 88% and that of C_1 is 67%, which signify that active surface molecules in C_2 are hig[her] than the C_1. This is also corroborated from the observed higher roughness of C_2 (Figure S11 and Figure S8). Generally it [is] observed that for an increase in charge-discharge cycle th[e] coulombic efficiency gradually decreases after certain time due to the structural changes. For C_1 nanosheet,, coulomb[ic] efficiency gradually decreases only after 800 cycles and becomes fixed at 81% through 7000 cycles. After that η value[s] decreases to 76% and becomes fixed up to 10000 cycles. Bu[t] for C_2, the coulombic efficiency remains almost 100% till 800[0] cycles. After 8000 cycles coulombic efficiency decreases t[o] 94% and becomes fixed up to 10000 cycles. This discrepanc[y] occurs for C_1 due to the ruptured structure during the charg[e] discharge cycle at higher current density but for C_2, th[e] structure remains intact indicating the inherited robustness [of] the nanosheet due to the presence of vanadium oxide i[n] $Co_3V_2O_8$ matrix. Presence of vanadium oxide provides a structural support to the $Co_2V_2O_8$ matrix.[14] TEM images o[f] and C_2 after 10000 cycles (Figure S12) also confirm the interpretation in the discussion. From the above discussion it is evident that the superior electrochemical activity of th[e] $Co_3V_2O_8$ is due to the synergistic effect of binary metal oxid[e] (Co and V).[14,15] In recent days, researchers use curre[nt] collectors like Ni foam[6,8,22,29] or carbon fiber[27] having larg[e] surface area to get high specific capacitance value fo[r] supercapacitor material. In our case we used glassy carbon a[s] the working electrode whose surface area is very small than the carbon fiber or Ni foam, yet the materials showed specif[ic] capacitance value superior to most of the reported direct and indirect nanostructured electrodes.[6,8,22,29] Figure 3d demonstrates the Ragone plot (energy density vs. pow[er] density). Here, we can see that power density of C_1 sample i[s] comparable to C_2 but energy density is quite low than C_2. Here in our case C_2 shows energy density 209.66 Wh kg^{-1} and powe[r] density 302.3 W kg^{-1} at 1 A/g current density, again at 30 A/g energy density is 70 Wh kg^{-1} and power density is 9420.56 W kg^{-1}. On the other hand, C_1 shows energy densities 62.8 and 23.05 Wh kg^{-1} at power densities 300.53 and 8865.38 W kg^{-1} at 1 A/g and 30 A/g current density, respectively. Interestingly,

for C_2 energy density is very much competitive with the Li-ion batteries and much higher than the reported supercapacitors (Table S3 demonstrates the energy density of the reported pseudocapacitors).[2,34,35]

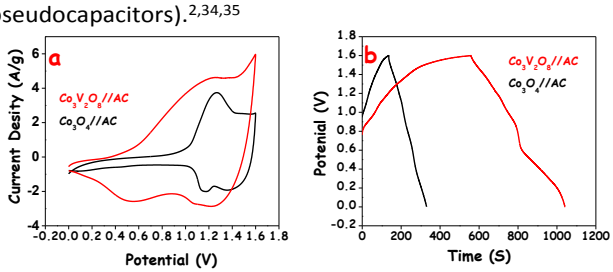

Fig. 4 (a) CV curve at 10 mV/S scan rate and (b) charge-discharge curve at 1 A/g current density for $Co_3V_2O_8$//AC and Co_3O_4//AC, respectively.

To support the electrochemical superiority of the as-synthesized nanosheets, electrochemical impedance spectroscopic (EIS) measurements (Figure S13) have also been done which is discussed briefly in the supporting information.

In order to investigate the practical utilization of the as-synthesized nanosheets (Co_3O_4 and $Co_3V_2O_8$), asymmetric two electrode cell has been developed where Co_3O_4 and $Co_3V_2O_8$ were used as the positive electrode and activated carbon (AC) was used as the negative electrode. Fabrication of the asymmetric cell for both samples has been discussed in the supporting information. Figure 4 illustrates the CV curves and charge discharge curve for both the two electrode cells, Co_3O_4//AC and $Co_3V_2O_8$//AC. Redox peaks in the CV curves for both samples indicate the pseudocapacitive nature of the asymmetric supercapacitor. Charge-discharge plot, stability with cycles, Nyquist plot and Ragone plot have been discussed in the supporting information for both the assembled cells. Specific capacitance value of Co_3O_4//AC and $Co_3V_2O_8$//AC assembled cells are 121 F/g and 303 F/g, respectively at 1 A/g current density. Due to the superior specific capacitance values and high voltage window (1.6 V), energy density values of the asymmetric supercapacitors are also very high (43.09 Wh kg^{-1} for Co_3O_4//AC and 107.95 Wh kg^{-1} for $Co_3V_2O_8$//AC).

In summary, we, for the first time, have described the importance of strong ammonia mediated hydrolysis under MHT for the synthesis of two ultrathin 2D cobalt oxide nanosheets with superior electrochemical activity. The as-synthesized Co_3O_4 with its 2D ultrathin nanosheet structure has proved to be a very efficient pseudocapacitor material. Then judicious insertion of robust vanadium oxide, considering its multiple oxidation states, into Co_3O_4 matrix makes it an extraordinary pseudocapacitor, $Co_3V_2O_8$. Especially, the as-synthesized $Co_3V_2O_8$ nanosheet shows high specific capacitance value, excellent structural stability, and electrochemical stability after extended charge-discharge cycles. Above all, energy density of $Co_3V_2O_8$ is very high and remarkably competitive to the Li-ion battery and other reported super capacitors.

The authors are thankful to DST, India and CSIR, New Delhi for financial assistance, Prof. Kumar Biradha, Department of Chemistry, IIT Kharagpur for BET measurement and IIT Kharagpur for instrumental support.

Notes and references

1 J. R. Miller andP. Simon, *Science*,2008, **321**, 651.
2 S. Gao, Y. Sun, F. Lei, L. Liang, J. Liu, W. Bei, B. Pan and Y. Xie, *Angew. Chem. Int. Ed.*,2014, 53, 12789.
3 S. K. Meher, P. Justin, and G. R.Rao, *Nanoscale*, 2011, **3**, 683
4 Y. K. Hsu, Y. C.Chen, Y. G.Lin, L. C. Chen andK. H. Chen,*Chem. Commun.*,2011, **47**, 1252.
5 G. W.Yang, C. L. XuandH. L. Li, *Chem. Commun.*, 2008, **48**, 6537.
6 D. Yan, H. Zhang, L. Chen, G. Zhu, S. Li, H. Xu and A. Yu, *ACS Appl. Mater. Interfaces*,2014, **6**, 15632.
7 L. Cao, F. Xu, Y. Y. Liang, H. L. Li, *Adv. Mater.* **2004**, *16*, 1853-1857.
8 H. Xia, D. Zhu, Z. Luo, Y. Yu, X. Xhi, G. Yuan, J. Xie, *Sci. Rep.*, 2013, **3**, 2978.
9 C. Mondal, A. K. Sasmal, S. M. Yusuf, M. D. Mukadam, J. Pal, M. Ganguly and T. Pal, *RSC Adv.*,2014, **4**, 56977.
10 M. Xing, L. B. Kong, M. C. Liu, L. Y. Liu, L. Kang and Y. C. Luo, *J.Mater. Chem. A*,2014, **2**, 18435.
11 Y. Zhao, Y.Liu, X.Du, R. Han and Y. J. Ding, *J. Mater. Chem.* 2014, **2**, 19308.
12 G. Yang, C. Cui, G. Yang and Wang, C. *ACS Nano*, 2014, **8**, 4474.
13 Y. Zhang, Y. Liu, J. Chen, Q. Guo, T. Wang and H. Pang, *Sci. Rep.,* 2014, **4**, 5687.
14 B. Saravanakumar, K. K. Purosothaman and G. Muralidharan, *CrystEngComm,* 2014, **16**, 10711.
15 F. K. Butt, M. Thair, C. Cao, F. Idrees, R. Ahmed, W. S. Khan, Z. Ali, N. Mahmood, M. Tanveer, A, Mahmood and I, Aslam *ACS Appl. Mater. Interfaces*, 2014, **6**, 13635.
16 Q. Li, N. Mahmood, J. Zhu, Y. Hou and S. Sun, *Nano Today,* 2014, **9**, 668.
17 N. Mahmood, C. Zhang, H. Yin and Y. Hou, *J. Mater. Chem. A,* 2014, **2**, 15 .
18 A. K. Sinha, S. Jana, S. Pande, S, Sarkar, M. Pradhan, M. Basu, S. Saha, A. Pal and T. Pal, *CrystEngComm.*,2009, **11**, 1210.
19 A. K.Sinha, M. Pradhan and T. Pal, *J. Phys. Chem. C*, 2013, **117**, 23976.
20 F. Wang and X. Wang, *Nanoscale*, 2014, **6**, 6398.
21 C. Wang, G. Du, K. Stahl, H. Huang, Y. Zhong and J. Z. Jiang, *J. Phys. Chem. C,* 2012, **116**, 4000.
22 Q. Guan, J. Cheng, B. Wang, W. Ni, G. Gu, X. Li, L. Huang, G Yang and F. Nie, *ACS Appl. Mater. Interfaces*,2014, **6**, 7626.
23 L.Wang, C.Lin, F. ZhangandJ. Jin, ACS Nano,2014, **8**, 3724.
24 S. K. MeherandG. R. Rao, *J. Phys. Chem. C*,2011, **115**, 25543.
25 Y. Zhu, C. Cao, S. Tao, W. Chu, Z. Wu and Y. Li, *Sci. Rep.*2014, **4**, 5787.
26 N. Mahmood, M. Tahir, A. mahmood, J. Zhu, C. Cao and Y. Hou,*Nano Energy*,2015, **11**, 267.
27 L. Q. Mai, A. M. Khan, X. Tian, K. M. Hercule, Y. L. Zhao, X. Li and X. Xu, *Nat. Commun.*, 2013,**4**, 2923.
28 C. Zhao, W. Zheng, X. Wang, H. Zhang, X. Cui and H. Wang,*Sci. Rep.*2013, **3**, 2986.
29 S. K. Meher, and G. R. Rao, J. Phys. Chem. C,2011, **115**, 15646.
30 X. H. Xia, J. P. Tu, X. L. Wang, C. D. Gu and X. B. Zhao, *Chem Commun.*, 2011, **47**, 5786
31 X. Wang, M. Li, Z. Chang, Y. Yang, Y. Wu and X. liu, *ACS Appl. Mater. Interfaces*, 2015, **7**, 2280.
32 S. He and W. Chen, *Nanoscale*, 2015, **7**, 6957.
33 N. Mahmood, M. Tahir, A. Mahmood, W. Yang, X. Gu, C. Cao Y. Zhang and Y. Hou, *Sci. China Mater.,* 2015, 58: 114–125
34 A.Pendashteh, M. S. Rahmanifar, R. B. Kaner and M. F. Mousav,*Chem. Commun.*, 2014, **50**, 1972.
35 H. Jiang, J. Ma and C. Li, *Chem. Commun.*, 2012, **48**, 4465.